

1 Combined Raman and Turbidity Probe for Real-Time Analysis of 2 Variable Turbidity Streams

3 Amanda M. Lines,* Job M. Bello, Christina Gasbarro, and Samuel A. Bryan*



Cite This: <https://doi.org/10.1021/acs.analchem.1c05228>

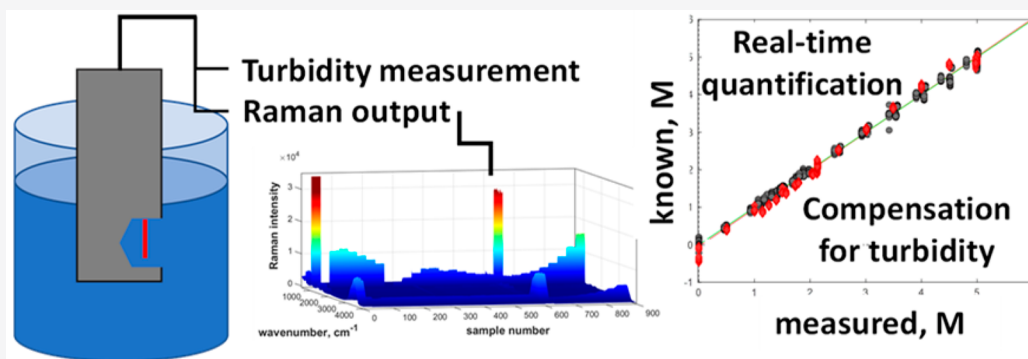


Read Online

ACCESS |

Metrics & More

Article Recommendations



4 **ABSTRACT:** Real-time and *in situ* process monitoring is a powerful tool that can empower operators of hazardous processes to
5 better understand and control their chemical systems without increased risk to themselves. However, the application of monitoring
6 techniques to complex chemical processes can face challenges. An example of this is the application of optical spectroscopy,
7 otherwise capable of providing detailed chemical composition information, to processes exhibiting variable turbidity. Here, details on
8 a novel combined Raman spectroscopy and turbidimetry probe are discussed, which advances current technology to enable flexible
9 and robust *in situ* monitoring of a flowing process stream. Furthermore, the analytical approach to accurately account for both
10 Raman signal and turbidity while quantifying chemical targets is detailed. This new approach allows for accurate analysis without
11 requiring assumptions of stable process chemistry, which may be unlikely in applications such as waste cleanup. Through leveraging
12 Raman and turbidity data simultaneously collected from the combined probe within chemometric models, accurate quantification of
13 multiple chemical targets can be achieved under conditions of variable concentrations and turbidity.

14 ■ INTRODUCTION

15 The integration of online monitoring technology represents a
16 key feature of modernization and advancement of all manners
17 of chemical processing fields.^{1–4} This is particularly true in
18 chemical processes where harsh conditions or hazards from the
19 process streams make traditional grab sample collection
20 challenging or extremely expensive. A key example of this is
21 nuclear waste cleanup, a major activity at environmental
22 superfund sites such as Hanford.^{3,5,6}

23 Numerous forms of online monitoring could be integrated
24 to give insight into process flow dynamics, vessel integrity, or
25 other key process features. Of particular interest to this work is
26 the monitoring of the chemical composition of a process
27 stream, information that is needed to control product quality,
28 improve process efficiency, maintain operation safety param-
29 eters, or demonstrate regulatory compliance. Again, a number
30 of instruments can provide this type of process character-
31 ization, and likely, a comprehensive tool will require the
32 combination of multiple sensor types. However, an ideal piece
33 of the process characterization system is optical spectroscopy.

34 Various optical approaches are already leveraged in food
35 processing or pharmaceutical production and can provide a
36 unique insight into the chemical composition of a stream, not
37 only identifying and quantifying chemical targets but also
38 enabling analysis of oxidation states, speciation, and complex
39 chemical interactions.^{7–9}

40 Recent advances in data analysis approaches have enabled
41 the application of optical spectroscopy-based monitoring
42 approaches under conditions that are traditionally prohibitive.
43 This includes applications where matrix effects,^{10–13} band
44 overlap,^{14–16} or baseline variation interferences^{17,18} are
45 present. This expansion of applications is largely due to the
46 utilization of multivariate analysis approaches such as chemo-

Received: December 2, 2021

Accepted: February 7, 2022

metric analysis.^{19–21} However, advances in optical probe materials have also allowed for deployments in radioactive environments,⁶ highly corrosive processes,^{16,22} or high temperature systems such as molten salts.^{16,23} Furthermore, the incorporation of sensor fusion into probe design has also expanded the applicability of optical spectroscopy.^{24–26}

There are several limitations in quantitative optical techniques that are common to essentially all forms of Raman measurement. These challenges include (1) absorption of Raman laser excitation by one or more constituents causing a decrease in signal;²⁷ (2) solute–solute interactions causing an increase in the number of degrees of freedom in the system, which is manifested in additional chemical components;¹⁸ (3) photochemistry induced by the excitation laser causing chemical changes to components, adding additional complexity in the system;²⁸ (4) excitation laser inducing fluorescence from either primary analyte or unknown interferences in the system, increasing baseline noise or shifts/changes/new bands in the Raman spectrum.²⁹ Many of these challenges have been addressed in other papers while this work focuses on a final and common challenge: (5) solutions can be complex in composition having inhomogeneity with particles causing scattering by either completely scattering away from the detector or partial scattering of light causing an increase in path length.³⁰ Addressing this effect of increased turbidity on blocking/scattering excitation light on the Raman measurement and allowing for the modular integration of Raman into large scale for variable turbidity process streams are significant needs.

Here, we demonstrate how chemometric analysis and sensor fusion can be combined to expand optical-based monitoring approaches into process conditions that traditionally limit monitoring success: variable turbidity streams. Specifically, the development and demonstration of a combined Raman–turbidity measurement probe is described. Several previous works discuss methods for overcoming turbidity impacts, where work discussed here advances both the probe design and analytical approach to new applications.^{31–33} The combined Raman–turbidity probe allows for a unique opportunity to relate changes in Raman response to changes in turbidity of the sample or process stream through simultaneous data collection. Chemometric models that incorporate both data streams are then uniquely capable of accounting for effects and quantifying target chemical species. Two points of advancement and novelty are covered by this work: (1) the compact probe design allows for flexible *in situ* monitoring directly on a process stream or batch, and (2) the analytical approach can avoid assumptions of stable chemistry that may hinder accurate applications to dynamic process streams.

EXPERIMENTAL SECTION

Materials. Reagents, NaNO_3 , NaNO_2 , and Na_2SO_4 , were procured from Sigma and used as received. Solutions were prepared using 18 M Ω -cm deionized water. Turbidity standards (Hach) were formazin stock suspension/solution and were added to training and validation sample/flow sets to achieve variable turbidity.

Instrumentation. The Raman spectrometer was an InPhotonics system employing a CCD detector and using a 670 nm, 300 mW, single mode laser (Process Instruments). This system was integrated with multichannel silicon detectors for turbidity measurement. Spectral data was collected and passed through a processing algorithm on the ratio of signals

from the multichannel measurement points to output turbidity. This analysis system was calibrated using 5 turbidity standards covering a range of 0 to 1000 NTU prior to each experiment. NTU (Nephelometric turbidity unit), while not an SI unit, is used extensively in the fields of water quality and used for the estimation of water clarity and/or selected characteristics of suspended sediment.^{34,35}

Probe Design and Flow Loop Configuration. The combined Raman–turbidity probe was developed by EIC Laboratories (Norwood, MA) through a small business innovative research (SBIR) grant. A picture of the probe can be seen in Figure 1A. The optical property of turbidity is the

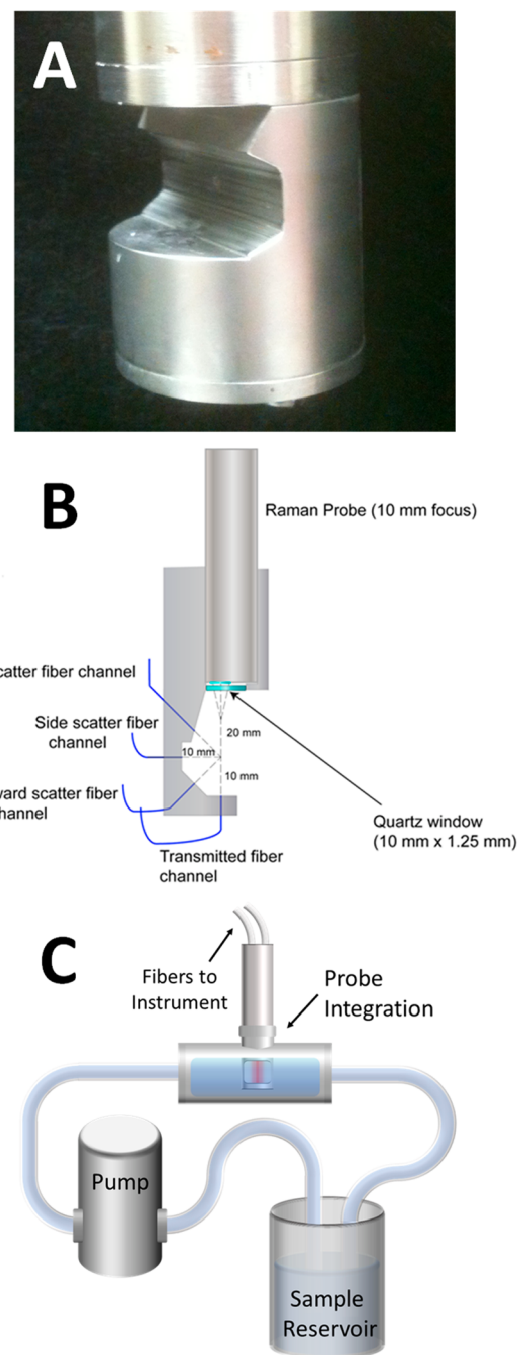


Figure 1. (A) Picture of combined Raman–turbidity probe, (B) training set collection configuration, and (C) flow loop configuration.

121 interaction between light and suspended particles in solution,
122 where the sample scatters light on the basis of the size, shape,
123 and composition of the particles as well as the wavelength of
124 the incident light. The intensity of the scattered light collected
125 at different angles can be calibrated to provide particle
126 concentration and size information using a well established
127 optical scattering theory.³⁶ In this design, the dual (Raman–
128 turbidity) sensor utilizes EIC's miniature Raman fiber optic
129 probe (671 nm laser excitation) for Raman excitation and
130 collection as well as provides the excitation source for the
131 turbidity sensor. The backscattering Raman probe is fixed
132 above the turbidity sensing region. The focus of the Raman
133 probe was adjusted to the edge of the radius of the 10 mm
134 circle collection region of the turbidity sensor. Four fiber optic
135 channels were arranged at different angles around the light
136 scattering collection radius. These turbidity collection angles
137 are 180° (transmitted), 135° (forward scatter), 90° (side
138 scatter), and 45° (back scatter); see Figure 1B. The optical
139 fibers are all equidistant (10 mm) from the center of the
140 turbidity collection circle. Turbidity was calculated by ratioing
141 the intensity of light between the four channels ($I_{45}/[I_{45} + I_{90} +$
142 $I_{135} + I_{180}]$) and calibrating the result to the turbidity
143 standards. Standards were procured and used as received
144 from Hach (0, 20, 200, 1000, and 4000 NTU). These
145 formazin-based standards can exhibit a random particle size
146 distribution from <0.1 to >10 μm with varying particle
147 conformations.

148 The probe was used to collect training sets, measuring both
149 Raman signal and turbidity, in static sample vessels; see Figure
150 1B. It was then integrated into a flow loop to measure flowing
151 systems; see Figure 1C.

152 **Chemometric Modeling.** Data analysis was completed
153 using MATLAB version 9.7.0.1190202 (R2019b), and chemo-
154 metric modeling was completed using The PLS Tool Box
155 version 8.7.1 from Eigen vector Research Inc. Details on model
156 parameters and metrics are supplied in the Results and
157 Discussion.

158 ■ RESULTS AND DISCUSSION

159 **Turbidity Impacts on Raman Signal.** The combination
160 of the capability to measure both Raman spectroscopy and
161 turbidity into a single probe produces a tool that can be highly
162 valuable to process characterization and control. As an
163 example, this opens new opportunities in nuclear waste
164 remediation. Raman is a well-known technique that can be
165 used to identify and quantify a long list of chemical species that
166 comprise the majority of Cold War-era nuclear wastes by
167 mass.³ Furthermore, Raman has already been utilized to
168 quantify multiple analytes in real waste processing samples
169 from the Hanford site.^{6,33} In this application, Raman is an ideal
170 approach because of the known optical activity of multiple
171 analytical targets in the waste and also because of the ease of
172 remote deployment.^{3,6} However, methods discussed here
173 could be modified to support other optical approaches.

174 However, with standard probe design, Raman can be
175 difficult to apply to streams of variable turbidity. Figure 2A
176 presents a picture of turbidity standard solutions, comparing a
177 0 NTU (completely clear) solution to a series of solutions at
178 increasing NTU values. As can be seen, the increasing turbidity
179 disrupts optical clarity. In the case of Raman, the increase in
180 turbidity causes significantly more light to be scattered and
181 results in a decrease of the overall signal intensity. Figure 2B
182 also demonstrates how the signal of nitrate, a very common

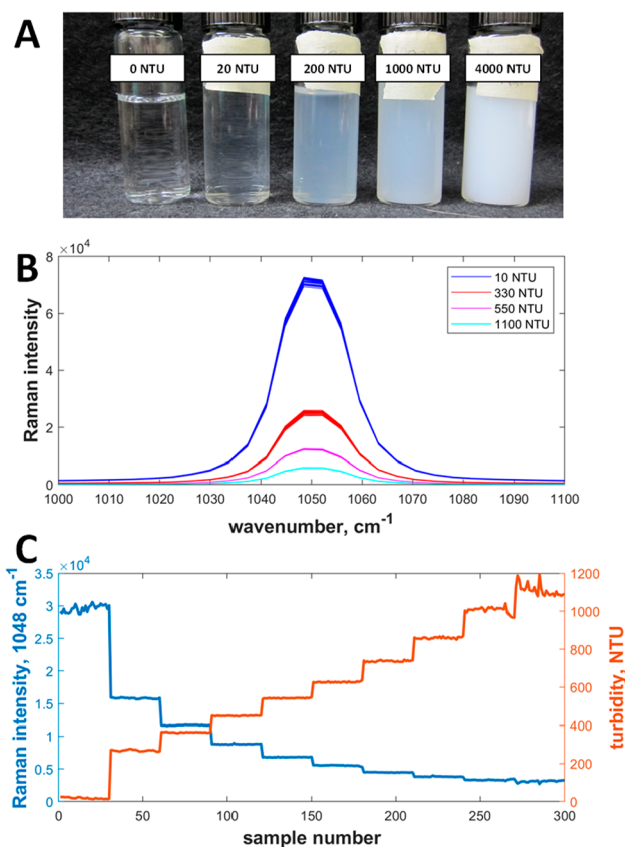


Figure 2. (A) Picture of samples at 0, 20, 200, 1000, and 4000 NTU. (B) Plot of Raman data for a series of solutions with a constant nitrate concentration (5 M) as turbidity increases and (C) a double axis plot showing the simultaneous measurement results of measuring turbidity and Raman intensity of the nitrate band.

183 waste species, drops as solution turbidity increases. The
184 simultaneous measurement of turbidity provides insight into
185 this behavior, which can also be seen in Figure 2C. As turbidity
186 is stepped up, overall Raman signal steps down even when the
187 nitrate concentration is constant.

188 The increase of turbidity acts roughly like a neutral density
189 filter. The signal decrease across the entire Raman spectrum is
190 roughly constant, so while intensity decreases, ratios between
191 bands remain constant.

192 **Advanced Quantification in the Presence of Variable**
193 **Turbidity.** The data complexity resulting from both variable
194 concentrations and variable turbidity lead to a situation where
195 single variate analysis approaches will be difficult to accurately
196 apply. Band intensity can no longer be solely related to the
197 concentration of target analyte. Further complexity is added
198 when considering the presence of additional chemical species
199 with interfering bands. Under these conditions, multivariate
200 approaches such as chemometric analysis are needed to
201 accurately and quickly process data with any confidence.
202 Chemometric analysis has been successfully applied to the
203 analysis of multicomponent solution streams with accordingly
204 complex Raman data.^{6,10,11,22} The general behavior of the
205 Raman signal as a function of increasing turbidity (i.e., the
206 consistency of band ratios) initially suggests previously
207 demonstrated modeling approaches could be leveraged. In
208 these cases, normalization was used to account for modulations
209 in overall band intensity caused by changes in laser power or

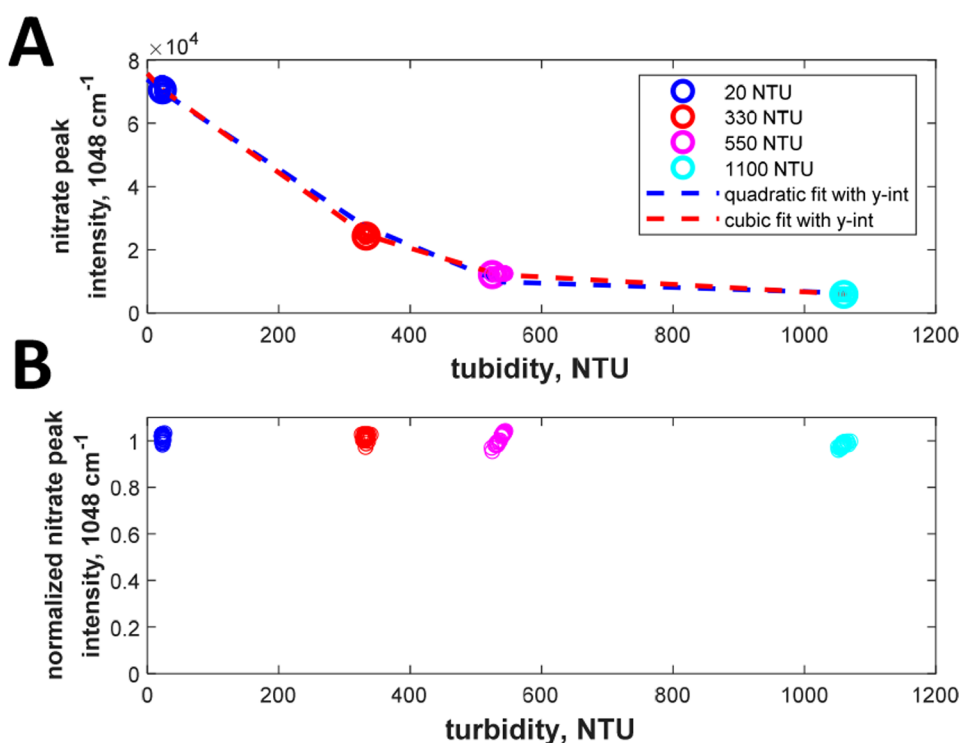


Figure 3. For solutions at constant 5 M NO_3^- and increasing turbidity: (A) plotted Raman intensities of the nitrate band (spectra shown in Figure 2B) showing the fit of data regression for eqs 1 and 2; (B) Raman intensities of nitrate bands after applying eq 3 and normalizing for turbidity.

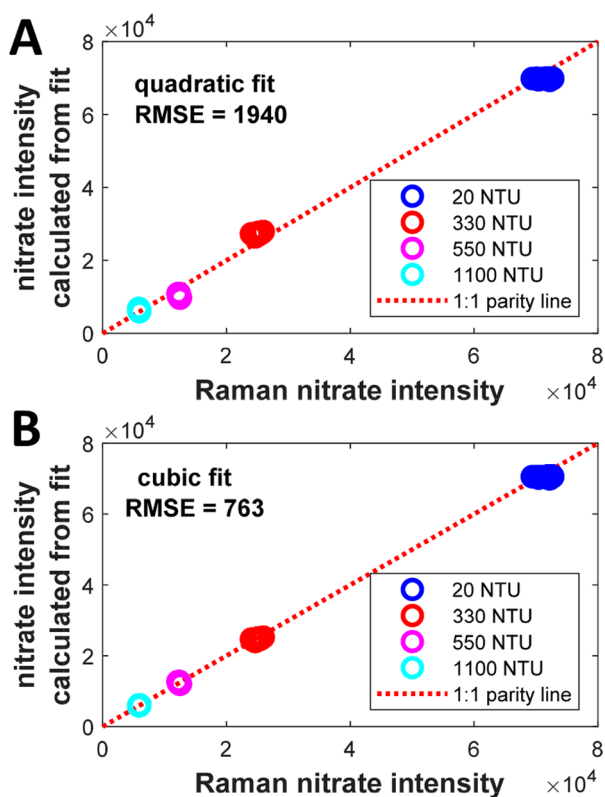


Figure 4. Comparison of the fitted intensities vs known intensities comparing fits using (A) quadratic eq 1 and (B) cubic eq 2 for the Raman intensities of 5 M nitrate samples as a function of turbidity.

accomplish this. However, when one plans for applications to treat legacy nuclear waste, monitoring approaches must be prepared for highly complex process streams (>10 optically active or interfering species present and very high ionic strength solutions) where the variability of the water band prohibits reliable normalization. Without an internal standard, this optical complexity makes it difficult to apply a normalization without introducing a new error artifact.

Directly accounting for turbidity within the chemometric model is the best route to accurately compensate for variable turbidity.

The first challenge is determining how to best integrate turbidity data within models. Appending turbidity measurements to Raman data through multiblock modeling approaches is one option, but it carries the risk of underrating the importance of turbidity to the analysis. This is particularly clear when comparing turbidity measurements (typically 1000 NTU or less), which are unidimensional (rank 1) to Raman spectral data (with peak intensities >3000 counts), which are multidimensional (high rank in latent variables). Weighting the various blocks can be used to mitigate this but can be challenging in cases with different underlying latent variable dimensionalities,³⁷ as was the case here, and our simplistic attempts at this still saw an underrating of turbidity impact.

A straightforward alternative that can also provide valuable insight into the optical impacts of turbidity is to normalize Raman results by turbidity values. To explore this pathway, the Raman peak intensity of the NO_3^- band in 5 M solutions was plotted across a range of turbidity values. Figure 3A presents this and indicates a nonlinear relationship between Raman signal and turbidity. To determine the best mechanism for turbidity normalization, several curves were fitted to build regression coefficients for intensity based on nitrate intensity

the presence of light absorbing species.¹³ In relatively simple chemical systems, normalization to the water band can

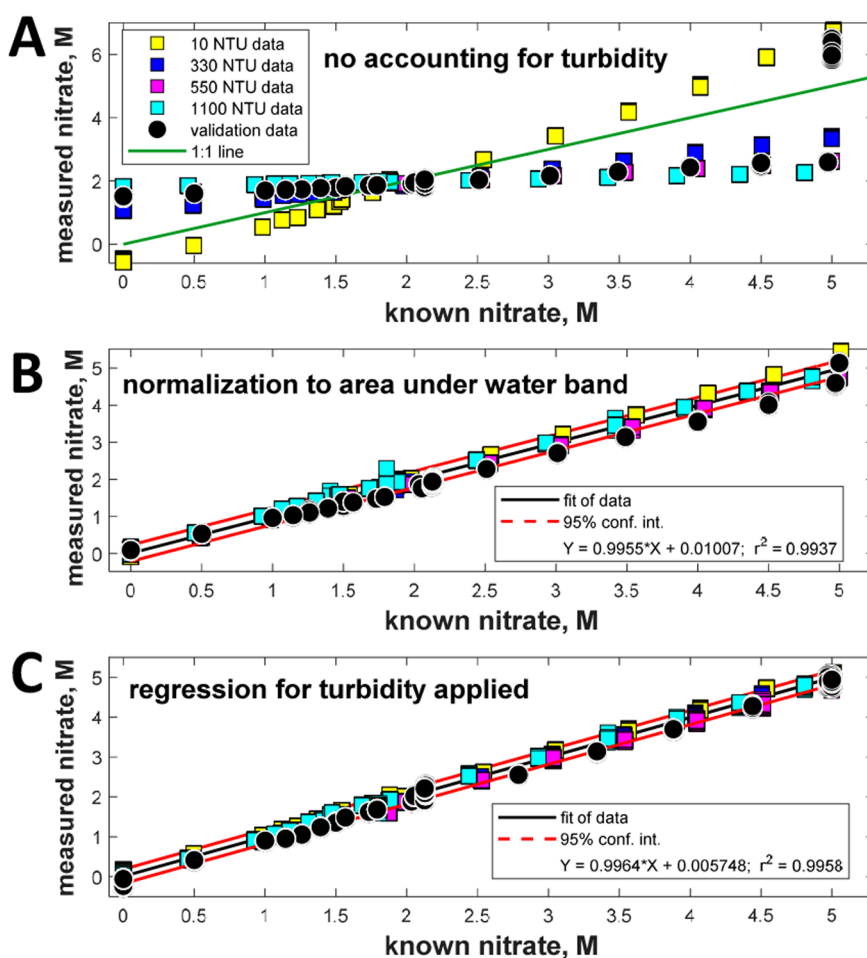


Figure 5. Parity plots of PLS models built by (A) not accounting for turbidity, (B) normalizing to the water band, and (C) applying the turbidity regression, eq 3, to the data prior to model building.

Table 1. Model Details and Metrics Including Number of Latent Variables (LVs) and R^2 of Fits to Both Calibration (cal) and Validation/Prediction (pred) Sets

analyte	model	LVs	RMSEC, RMSECV, RMSEP	R^2 of cal, pred
nitrate	not accounting for turbidity	2	0.92489, 0.96334, 0.87939	0.556, 0.521
	normalizing to water band	4	0.09869, 0.11000, 0.23182	0.995, 0.994
	normalizing using eq 3	4	0.08110, 0.08949, 0.13407	0.997, 0.996
nitrite	not accounting for turbidity	4	0.38233, 0.41698, 0.34066	0.555, 0.485
	normalizing to water band	4	0.03300, 0.04584, 0.05615	0.997, 0.994
	normalizing using eq 3	4	0.05283, 0.06018, 0.11533	0.992, 0.989
sulfate	not accounting for turbidity	4	0.10305, 0.11163, 0.08613	0.514, 0.445
	normalizing to water band	3	0.01692, 0.01821, 0.02445	0.986, 0.985
	normalizing using eq 3	2	0.01635, 0.01745, 0.00660	0.988, 0.986

regressed on turbidity using the quadratic and cubic equations shown in eqs 1 and 2, respectively:

$$y = a_0 + a_1x + a_2x^2 \quad (1)$$

$$y = b_0 + b_1x + b_2x^2 + b_3x^3 \quad (2)$$

where y represents the Raman intensity for the nitrate band (at 1048 cm^{-1}) and x represents the turbidity (in NTU units). The regression coefficients a_0 , a_1 , and a_2 from eq 1 are 73 826.79, 175.05, and 0.11, respectively, and the regression coefficients b_0 , b_1 , b_2 , and b_3 from eq 2 are 75 702.17, -228.95 , 0.26, and -0.00010 , respectively. The a_0 term from eq 1 and the corresponding b_0 term from eq 2 represent the Raman nitrate intensity (y) at zero turbidity units ($y = a_0$ or $y = b_0$ when $x = 0$). The mean Raman intensity for the lowest turbidity samples (~ 20 NTU) of the nitrate samples in Figure 3A is 71 666, which is expectedly slightly lower than the a_0 and b_0 values from the fit in eqs 1 and 2, owing to the slightly higher NTU value of these samples from zero.

The cubic fit (eq 2) was determined to best fit the data on the basis of the comparison of the fitted intensities vs known intensities by comparing the quadratic (eq 1) vs cubic (eq 2) fits of the Raman intensities of 5 M nitrate samples as a function of turbidity, as shown in Figure 4. The root-mean-square-error (RMSE) of the quadratic fit is 1940 compared to the RMSE for the cubic fit of 763. After normalizing the Raman data based on eq 3 (below), data could be replotted to show a constant Raman response for 5 M nitrate across a range of turbidity values (Figure 3B):

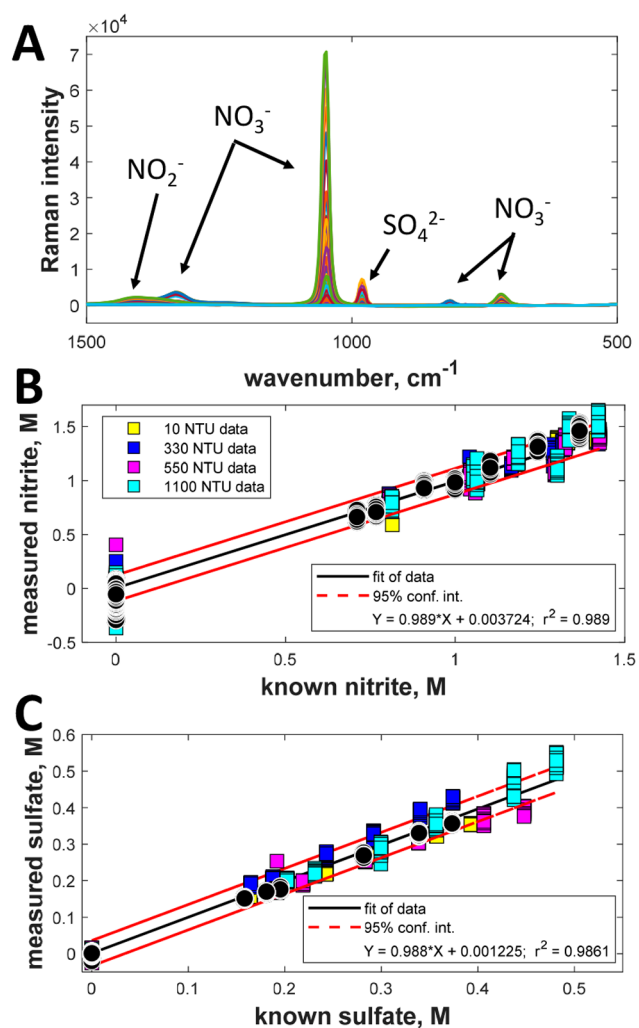


Figure 6. (A) Fingerprints of the three target species for the flow system and the parity plot showing the turbidity-inclusive model performance for the (B) NO_2^- and (C) SO_4^{2-} species.

$$Y_{\text{norm}(i,\lambda)} = \frac{Y_{(i,\lambda)}}{b_0 + b_1x_i + b_2x_i^2 + b_3x_i^3} \quad (3)$$

273 Y and Y_{norm} represent the matrix of the original Raman spectra
274 and normalized spectra, respectively, in which the intensities of
275 each wavenumber (λ) for each i^{th} spectrum is divided by the
276 cubic expression given in eq 2, and x_i is the turbidity value
277 measured for the sample represented by the i^{th} spectrum.

278 The spread of the data in the normalized nitrate peak
279 intensity increases at higher NTU values as observed in Figure
280 3B and is expected, since as the total Raman signal decreases
281 with increasing NTU while the absolute noise of the system is
282 expected to remain constant, the signal-to-noise ratio of the
283 Raman bands decreases. As the signal-to-noise decreases, the
284 relative error of analysis is then expected to increase, as can be
285 seen in the “normalized” data in Figure 3B. The sensitivity of
286 the results would be expected to be affected by this reduced
287 signal-to-noise caused by increases in turbidity. This can be
288 thought of in terms of the limit of detection (LOD) of the
289 analyte, as defined by the equation $\text{LOD} = 3 \times S_B/m$,³⁸ where
290 S_B is the standard deviation of the blank readings and m is the
291 slope of line obtained by plotting the intensity of the analyte
292 peak versus its concentration. As the signal is decreased in

solutions of increasing turbidity, the slope value (m) decreases,
293 while the measured blank samples, and therefore the standard
294 deviation of the blank (S_B), remain constant. This would lead
295 to an expected increase in the measured LOD (and decrease in
296 the sensitivity of the measurement) with increasing turbidity.

Chemometric Modeling. An optical training set was
298 collected to capture the fingerprints of nitrate, sulfate, and
299 nitrite across a range of concentrations and turbidities. For the
300 comparison of the performance, multiple modeling approaches
301 to account for turbidity were utilized. The first involved
302 normalizing data to the water band to account for signal
303 intensity dependencies on turbidity. Because this data set is
304 relatively simple chemically, normalization to the water band
305 will not introduce the same challenges as it would in real
306 nuclear waste samples. This approach can provide a baseline
307 for performance characterization. The second approach relied
308 on the normalization of data to turbidity by applying the
309 regression, eq 3. In addition to these approaches, modeling
310 without accounting for turbidity impacts was also completed to
311 provide insight into the magnitude of the impact of variable
312 turbidity to data complexity.

Data treated through both turbidity accounting methods was
314 then utilized to build chemometric models. Baseline effects in
315 the form of minor constant offsets were observed due to
316 variable light scattering in these solutions of variable turbidity.
317 A first derivative applied to each spectrum during preprocess-
318 ing was used as the primary means to remove these baseline
319 effects.¹⁹ In both cases, partial least squares (PLS) models were
320 used to correlate concentration to Raman signal.³⁹ Parity plots
321 comparing performance of the three modeling approaches for
322 NO_3^- are shown in Figure 5, and model parameters are
323 outlined in Table 1. Without accounting for turbidity, models
324 cannot effectively quantify nitrate (Figure 5A) and model
325 metrics such as the root-mean-square error of calibration
326 (RMSEC) and cross validation (RMSECV) show poor
327 performance. Accounting for turbidity by normalizing to the
328 area under the water band dramatically improves RMSECV,
329 which can be interpreted as a \pm error value on model outputs.⁴⁰
330 While these results indicate excellent model performance, it
331 should be emphasized that significant error can be introduced
332 into this approach if additional solution species impact the
333 shape of the water band.^{17,41} Significant improvement in model
334 performance is also observed when accounting for turbidity by
335 applying regression, eq 3. This route provides a more robust
336 approach to integrating turbidity impacts without building in
337 vulnerabilities to complex and changing solution composition.
338 Note, data shown in Figure 5 represents a combination of
339 nitrate-only samples and mixtures containing nitrate, nitrite,
340 and sulfate with compositions represented in Figures 6A and 7.
341 This provides a clear first step to compare and determine the
342 accuracy of the regression/modeling approach. This modeling
343 approach will be further tested in the following sections by
344 looking at models for nitrite and sulfate in multicomponent
345 mixtures to demonstrate performance in the conditions more
346 closely approximating waste treatment steps.

Data included in Table 1 shows the metrics of model
348 performance across a range of parameters as well as details of
349 the model specifications. This includes the number of latent
350 variables (LVs) used by the model as well as RMSEC,
351 RMSECV, and RMSEP. Overall, LVs were kept low to avoid
352 model overfitting, and root-mean-square errors were roughly
353 similar, internal to each model, indicating robust models. It
354 should be noted that error or uncertainty in model outputs can
355

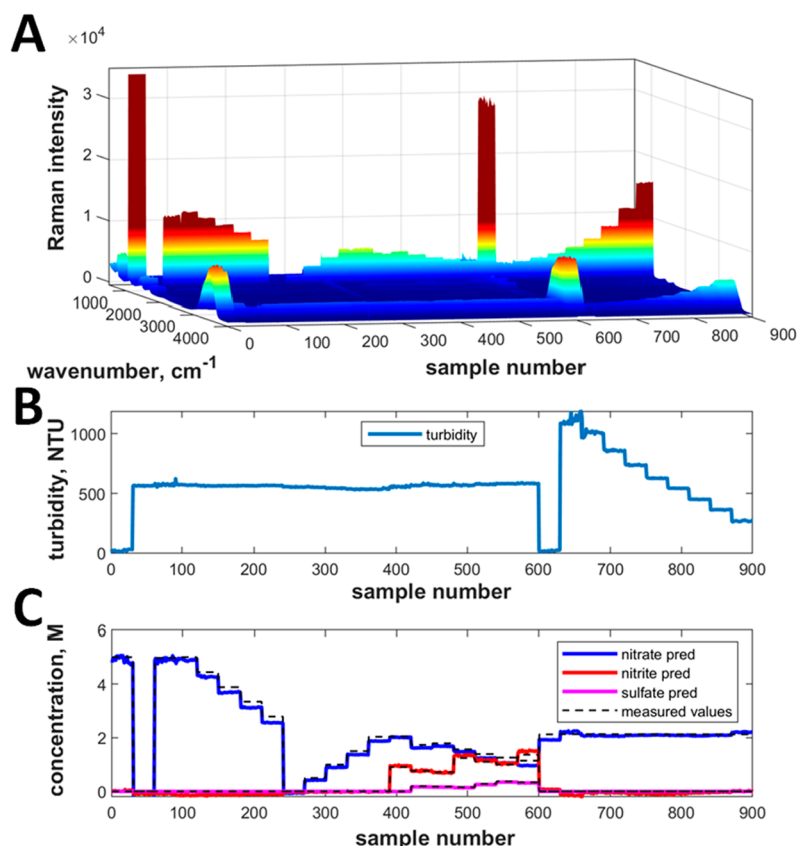


Figure 7. Plot showing (A) Raman signal and (B) measured turbidity over the course of the flow test and (C) the chemometric model results for quantification.

356 be roughly interpreted as $\pm\text{RMSECV}$.⁴⁰ Here, those errors
357 were relatively low compared to the analyte concentration
358 ranges, indicating accurate model performance.

359 **Flow Test Demonstrations and Validation.** To simulate
360 the added complexity anticipated in real waste streams, a series
361 of flow tests were conducted. Not only did these add the
362 challenge of measuring a flowing stream while the training set
363 was collected on static solutions, but also three chemical
364 targets with interfering bands were simultaneously included,
365 NO_3^- , SO_4^{2-} , and NO_2^- , all of which were independently
366 varied. Finally, turbidity was varied to fully test chemometric
367 modeling accuracy in the presence of flowing streams,
368 interfering bands, varying concentrations, and varying
369 turbidity. Figure 6 presents the Raman fingerprints of the
370 target species along with parity plots for SO_4^{2-} and NO_2^-
371 where models were built after regressing data to turbidity.
372 Ideally, parity plots will show intercepts of zero and slopes of
373 unity with data fitting into confidence intervals. Near-zero
374 intercepts and near-unity slopes are observed in all models,
375 including those presented in Figures 5B,C and 6B,C. However,
376 in Figure 6B, while the fitted line has a near-zero intercept, the
377 predictions in the zero-nitrite data show a notable spread,
378 likely due to poorly defined latent variables (LVs) within the
379 model. This indicates higher uncertainty in nitrite results and
380 could likely be improved in future efforts by expanding the
381 nitrite training set.

382 Raman signals and turbidity that were measured during the
383 flow run are presented in Figure 7. During the flow run,
384 standards would periodically be added to the flow loop. The
385 system would be allowed to reach equilibrium, and then,

386 conditions would be held constant for several minutes before
387 the next addition of a standard. Periods of varying target
388 concentration and varying turbidity are labeled in Figure 7B,C.
389 As anticipated, intensity fluctuations of bands are observed
390 with both changing concentration and turbidity. This provides
391 a clear demonstration of data complexity that challenges the
392 accurate measurement of target concentrations under variable
393 turbidity and solution composition.

394 Models were applied to collected data and resulting
395 measurements of concentration are shown in Figure 7C.
396 Overall, through accounting for turbidity, models are able to
397 accurately quantify all three targets despite variable concen-
398 tration and turbidity. It is notable that the training data set
399 used to establish the turbidity correction (eqs 2 and 3)
400 contained only a limited number of samples consisting of one
401 concentration of nitrate (5 M) at four NTU values (~ 20 , 330,
402 550, and 1100), while the validation data in Figure 7 (which
403 was not utilized to build the model) includes NTU values that
404 ranged from ~ 20 to ~ 1100 NTU in increments of ~ 100 NTU
405 units. This approach can provide significant insight into the
406 chemical composition and behavior within complex processing
407 streams, enabling real-time process control and optimization.
408 This system captures the complexities of variable 3-component
409 concentrations and turbidity. While this is a robust training
410 and demonstration system, the expansion to solution
411 conditions with >5 target analytes will begin to better
412 approximate real waste conditions. This monitoring and
413 analytical approach can be transitioned to those higher
414 complexity systems using approaches described previ-
415 ously.^{6,42,43}

416 Furthermore, due to the particle size and shape distribution
417 common to formazin standards, these results indicate this
418 approach can be applied to systems with variable particle
419 morphologies. Note, particles of different color or reflectivity
420 would further impact the spectrum, resulting in reductions of
421 signal (for dark particles) or changes in baselines shape (more
422 reflective particles). The data preprocessing algorithms used
423 here, normalization and a first derivative, should also account
424 for these variations in signal. Overall, the approach described
425 here should be widely applicable to turbid streams.

426 ■ CONCLUSION

427 The combined Raman–turbidity probe described here was
428 able to simultaneously measure two key aspects of solution
429 behavior. Raman spectroscopy was able to successfully identify
430 the unique fingerprints of the chemical species present: nitrate,
431 nitrite, and sulfate. Turbidimetry was able to successfully
432 measure the optical clarity of the solution. However, the
433 increase in turbidity resulted in a decreased Raman signal,
434 making quantification of the chemical species difficult to
435 complete accurately. When Raman output was regressed by
436 measured turbidity, data sets could be used to build accurate
437 chemometric models for the quantification of chemical targets
438 under conditions of both variable concentration and turbidity.
439 This was demonstrated in a complex flow sheet and lays the
440 foundation for the integration of combined Raman and
441 turbidity monitoring into complex, variable turbidity processes.

442 ■ AUTHOR INFORMATION

443 Corresponding Authors

444 **Amanda M. Lines** – Pacific Northwest National Laboratory,
445 Richland, Washington 99354, United States; Phone: 509-
446 375-5689; Email: amanda.lines@pnnl.gov

447 **Samuel A. Bryan** – Pacific Northwest National Laboratory,
448 Richland, Washington 99354, United States; [orcid.org/](https://orcid.org/0000-0002-8826-0880)
449 0000-0002-8826-0880; Phone: 509-375-5648;
450 Email: sam.bryan@pnnl.gov

451 Authors

452 **Job M. Bello** – Spectra Solutions, Inc., Norwood,
453 Massachusetts 02062, United States

454 **Christina Gasbarro** – Spectra Solutions, Inc., Norwood,
455 Massachusetts 02062, United States

456 Complete contact information is available at:

457 <https://pubs.acs.org/10.1021/acs.analchem.1c05228>

458 Notes

459 The authors declare no competing financial interest.

460 ■ ACKNOWLEDGMENTS

461 We thank Dr. Heather M. Felmy and Michael C. Perkins for
462 graphic design assistance. Research was supported in part by
463 the U.S. Department of Energy, Office of Science, through the
464 Small Business Innovative Research (SBIR) Program. This
465 work was performed at the Pacific Northwest National
466 Laboratory (PNNL), a multiprogram national laboratory
467 operated by Battelle for the U.S. Department of Energy.
468 PNNL is operated by Battelle Memorial Institute for the U.S.
469 Department of Energy under contract DE-AC05-76RL01830.

470 ■ REFERENCES

471 (1) Capodaglio, A. G.; Callegari, A. *Nato Sci. Peace Secur* **2009**, 153–
472 179.

- (2) McMullen, J. P.; Stone, M. T.; Buchwald, S. L.; Jensen, K. F. *Angew. Chem. Int. Edit* **2010**, 49 (39), 7076–7080. 473
- (3) Tse, P.; Bryan, S. A.; Bessen, N. P.; Lines, A. M.; Shafer, J. C. *Anal. Chim. Acta* **2020**, 1107, 1–13. 474
- (4) Zhang, Q. A.; Shen, Y.; Fan, X. H.; Yan, Y. Y.; Martin, J. F. G. *Cyta-J. Food* **2016**, 14 (3), 496–501. 475
- (5) Branch, S. D.; French, A. D.; Lines, A. M.; Rapko, B. M.; Heineman, W. R.; Bryan, S. A. *Environ. Sci. Technol.* **2018**, 52 (3), 1357–1364. 476
- (6) Lines, A. M.; Tse, P.; Felmy, H. M.; Wilson, J. M.; Shafer, J.; Denslow, K. M.; Still, A. N.; King, C.; Bryan, S. A. *Ind. Eng. Chem. Res.* **2019**, 58 (47), 21194–21200. 477
- (7) De Beer, T.; Burggraave, A.; Fonteyne, M.; Saerens, L.; Remon, J. P.; Vervaeet, C. *Int. J. Pharmaceut* **2011**, 417 (1–2), 32–47. 478
- (8) De Beer, T. R. M.; Vercruyssen, P.; Burggraave, A.; Quinten, T.; Ouyang, J.; Zhang, X.; Vervaeet, C.; Remon, J. P.; Baeyens, W. R. G. *J. Pharm. Sci.-Us* **2009**, 98 (9), 3430–3446. 479
- (9) De Beer, T. R. M.; Wiggenhorn, M.; Veillon, R.; Debacq, C.; Mayeresse, Y.; Moreau, B.; Burggraave, A.; Quinten, T.; Friess, W.; Winter, G.; Vervaeet, C.; Remon, J. P.; Baeyens, W. R. G. *Anal. Chem.* **2009**, 81 (18), 7639–7649. 480
- (10) Clifford, A. J.; Lackey, H. E.; Nelson, G. L.; Bryan, S. A.; Lines, A. M. *Anal. Chem.* **2021**, 93 (14), 5890–5896. 481
- (11) Lackey, H. E.; Nelson, G. L.; Lines, A. M.; Bryan, S. A. *Anal. Chem.* **2020**, 92 (8), 5882–5889. 482
- (12) Lines, A. M.; Adami, S. R.; Sinkov, S. I.; Lumetta, G. J.; Bryan, S. A. *Anal. Chem.* **2017**, 89 (17), 9354–9359. 483
- (13) Lines, A. M.; Hall, G. B.; Sinkov, S. I.; Levitskaia, T.; Gallagher, N. B.; Lumetta, G. J.; Bryan, S. A. *Ind. Eng. Chem. Res.* **2020**, 59, 8894–8901. 484
- (14) Lines, A. M.; Nelson, G. L.; Casella, A. J.; Bello, J. M.; Clark, S. B.; Bryan, S. A. *Anal. Chem.* **2018**, 90 (4), 2548–2554. 485
- (15) Nelson, G. L.; Asmussen, S. E.; Lines, A. M.; Casella, A. J.; Bottenus, D. R.; Clark, S. B.; Bryan, S. A. *Anal. Chem.* **2018**, 90 (14), 8345–8353. 486
- (16) Schroll, C. A.; Lines, A. M.; Heineman, W. R.; Bryan, S. A. *Anal. Methods-Uk* **2016**, 8 (43), 7731–7738. 487
- (17) Nelson, G. L.; Lackey, H. E.; Bello, J. M.; Felmy, H. M.; Bryan, H. B.; Lamadie, F.; Bryan, S. A.; Lines, A. M. *Anal. Chem.* **2021**, 93 (3), 1643–1651. 488
- (18) Nelson, G. L.; Lines, A. M.; Bello, J. M.; Bryan, S. A. *Acs Sensors* **2019**, 4 (9), 2288–2295. 489
- (19) Beebe, K. R.; Pell, R. J.; Seasholtz, M. B. *Chemometrics: A Practical Guide*; Wiley: New York, 1998. 490
- (20) Bro, R.; Elden, L. *J. Chemometr* **2009**, 23 (1–2), 69–71. 491
- (21) Gallagher, N. B.; Blake, T. A.; Gassman, P. L.; Shaver, J. M.; Windig, W. *Appl. Spectrosc.* **2006**, 60 (7), 713–722. 492
- (22) Felmy, H. M.; Clifford, A. J.; Medina, A. S.; Cox, R. M.; Wilson, J. M.; Lines, A. M.; Bryan, S. A. *Environ. Sci. Technol.* **2021**, 55 (6), 3898–3908. 493
- (23) Schroll, C. A.; Chatterjee, S.; Levitskaia, T. G.; Heineman, W. R.; Bryan, S. A. *Anal. Chem.* **2013**, 85 (20), 9924–9931. 494
- (24) Bryan, S. A.; Levitskaia, T. G.; Johnsen, A. M.; Orton, C. R.; Peterson, J. M. *Radiochim. Acta* **2011**, 99 (9), 563–571. 495
- (25) Lines, A. M.; Hall, G. B.; Asmussen, S.; Alfred, J.; Sinkov, S.; Heller, F.; Gallagher, N.; Lumetta, G. J.; Bryan, S. A. *Acs Sensors* **2020**, 5 (8), 2467–2475. 496
- (26) Nee, K.; Bryan, S. A.; Levitskaia, T. G.; Kuo, J. W. J.; Nilsson, M. *Anal. Chim. Acta* **2018**, 1006, 10–21. 497
- (27) Lines, A. M.; Hall, G. B.; Sinkov, S.; Levitskaia, T.; Gallagher, N. B.; Lumetta, G. J.; Bryan, S. A. *Ind. Eng. Chem. Res.* **2020**, 59 (19), 8894–8901. 498
- (28) Lai, C. W.; Schwab, M.; Hill, S. C.; Santarpia, J.; Pan, Y. L. *Opt. Express* **2016**, 24 (11), 11654–11667. 499
- (29) Zhao, J.; Lui, H.; McLean, D. I.; Zeng, H. *Appl. Spectrosc.* **2007**, 61 (11), 1225–1232. 500
- (30) Mupparapu, R.; Vynck, K.; Svensson, T.; Burreis, M.; Wiersma, D. S. *Opt. Express* **2015**, 23 (24), A1472–A1484. 501

- 541 (31) Barman, I.; Singh, G. P.; Dasari, R. R.; Feld, M. S. *Anal. Chem.*
542 **2009**, *81* (11), 4233–4240.
- 543 (32) Sinfield, J. V.; Monwuba, C. K. *Appl. Spectrosc.* **2014**, *68* (12),
544 1381–1392.
- 545 (33) Bryan, S. A.; Levitskaia, T. G.; Sinkov, S. I.; Schlahta, S. N.;
546 Shaver, J. M. Raman based process monitor for continuous real-time
547 analysis of high level radioactive waste components. In *Waste*
548 *Management Conference 2008: Phoenix Rising: Moving Forward in*
549 *Waste Management*, February 24–28, 2008, Phoenix, AZ; paper no.
550 8263.
- 551 (34) U.S. Geological Survey. *National Field Manual for the Collection*
552 *of Water-Quality Data (NFM)*; USGS, 2019; Chapter 6.7: Turbidity;
553 [https://www.usgs.gov/mission-areas/water-resources/science/](https://www.usgs.gov/mission-areas/water-resources/science/national-field-manual-collection-water-quality-data-nfm)
554 [national-field-manual-collection-water-quality-data-nfm](https://www.usgs.gov/mission-areas/water-resources/science/national-field-manual-collection-water-quality-data-nfm) (accessed
555 2022-01-12)
- 556 (35) ASTM. *Standard Test Method for On-Line Measurement of*
557 *Turbidity Below 5 NTU in Water*; ASTM D6698-07; ASTM, 2013;
558 <https://www.astm.org/d6698-07.html> (accessed 2022-01-12).
- 559 (36) Brumberger, H.; Stein, R. S.; Rowell, R. *Sci. Technol.* **1968**, *83*,
560 34–42.
- 561 (37) Campos, M. P.; Reis, M. S. *Chemometr Intell Lab* **2020**, *199*,
562 103959.
- 563 (38) Long, G. L.; Winefordner, J. D. *Anal. Chem.* **1983**, *55* (7),
564 712A–724A.
- 565 (39) Wold, S.; Sjostrom, M.; Eriksson, L. *Chemometr Intell Lab*
566 **2001**, *58* (2), 109–130.
- 567 (40) Faber, N. M.; Bro, R. *Chemometr Intell Lab* **2002**, *61* (1–2),
568 133–149.
- 569 (41) Nelson, G. L.; Lines, A. M.; Casella, A. J.; Bello, J. M.; Bryan, S.
570 *A. Analyst* **2018**, *143* (5), 1188–1196.
- 571 (42) Tse, P.; Shafer, J.; Bryan, S. A.; Lines, A. M. *Environ. Sci.*
572 *Technol.* **2021**, *55* (19), 12943–12950.
- 573 (43) Tse, P.; Shafer, J.; Bryan, S. A.; Nelson, G. L.; Lines, A. M. *Appl.*
574 *Spectrosc.* **2021**, 000370282110538.